UC Berkeley

UC Berkeley Previously Published Works

Title

Unlocking microbial access to amino-substituted 4-hydroxycoumarin derivatives via enzymatic promiscuity and metabolic engineering

Permalink

https://escholarship.org/uc/item/24t1n0cx

Journal

Metabolic Engineering, 99

ISSN

1096-7176

Authors

Zhao, Caiyi

Hou, Jingqi

Huang, Daphne

et al.

Publication Date

2027

DOI

10.1016/j.ymben.2026.102541

Copyright Information

This work is made available under the terms of a Creative Commons Attribution License, available at https://creativecommons.org/licenses/by/4.0/

Peer reviewed

eScholarship.org Powered by the California Digital Library
University of California

Unlocking Microbial Access to Amino-substituted 4-Hydroxycoumarin Derivatives via Enzymatic Promiscuity and Metabolic Engineering

Caiyi Zhao[1,2,3], Jingqi Hou[1,3,4], Daphne Huang[1,3,4], Cholapat Varongchayakul[1,3,4], Nuojin Cheng[1,3,4], Yilin Li[1,3,5], Chenyi Li[1,3,5]*, Jay D. Keasling[1,3,4,5,6,7]*

[1]Biological Systems and Engineering Division, Lawrence Berkeley National Laboratory, Berkeley, CA, USA;

[2]Department of Molecular and Cell Biology, University of California, Berkeley, CA, USA;

[3]Joint BioEnergy Institute, Emeryville, CA, USA;

[4]College of Chemistry, University of California, Berkeley, CA, USA

[5]California Institute for Quantitative Biosciences (QB3), University of California, Berkeley, CA, USA;

[6]Department of Chemical & Biomolecular Engineering, University of California, Berkeley, CA, USA;

[7]Department of Bioengineering, University of California, Berkeley, CA, USA.

*Correspondence: chenyiliucb@berkeley.edu; keasling@berkeley.edu

Abstract

Coumarins and their derivatives possess diverse bioactivities and broad applications in pharmaceuticals, food additives, and materials science. For example, amino-functionalized coumarin derivatives hold significant promise for the development of novel functional materials and drug discovery. However, the microbial biosynthesis of these compounds remains underexplored. In this study, we characterized the substrate flexibility of the type III polyketide synthase PqsD from *Pseudomonas aeruginosa* in *Pseudomonas putida* KT2440, showing its ability to convert various *para*- and *meta*-substituted salicylic acids into novel coumarin derivatives. Leveraging the substrate promiscuity of PqsD, we established a novel microbial route to produce 6-amino-4-hydroxycoumarin (6A4HC). Furthermore, we developed a new *de novo* biosynthetic route for its direct precursor, 5-aminosalicylic acid (5ASA), which is an FDA-approved pharmaceutical compound. This work expands the enzymatic toolbox for coumarin biosynthesis and highlights microbial platforms as sustainable alternatives for generating structurally diverse and functionalized coumarins.

Keywords: 6-amino-4-hydroxycoumarin, 5-aminosalicylic acid, *Pseudomonas putida*, Metabolic engineering, Enzyme promiscuity.

1. Introduction

Coumarin is a naturally occurring benzopyrone compound first isolated from the tonka bean (*Dipteryx odorata*) in 1820, and has since been identified in over 150 plant species across families such as Rutaceae, Umbelliferae, and Fabaceae (Sharifi-Rad et al., 2021; Vogel, 1820). Characterized by its fused benzene and alpha-pyrone ring system, coumarin and its derivatives exhibit a diverse range of physiological and biological properties that have sustained scientific interest for over two centuries (*Coumarin and its derivatives*, 2021). The conjugated π-electron system of the coumarin scaffold confers notable photophysical properties, including UV absorption and fluorescence, making it a compound of interest in optical and sensing applications (Cocco et al., 2021; Kaneko and Wang, 2024). Beyond their physical characteristics, coumarin and its structural analogs exhibit a broad spectrum of pharmacological activities—anticoagulant, anti-inflammatory, antimicrobial, antioxidant, and anticancer—largely owing to the versatility of the coumarin scaffold, which tolerates chemical modification at multiple positions (Annunziata et al., 2020; Balewski et al., 2021). Substituents can be introduced at C-3, C-6, C-7, and C-8 positions to enable the synthesis of thousands of derivatives with tailored properties for applications spanning medicinal chemistry and materials science (Al-Warhi et al., 2020; Balewski et al., 2021; Samanth and Bhat, 2024; Tang et al., 2024).

The global coumarin market is estimated at USD 219 million in 2026 and expected to rise to USD 370 million by 2035, with applications spanning pharmaceutical formulations (41% of consumption), fragrances and cosmetics (32% of consumption), and industrial uses such as electroplating and optical brighteners ("Coumarin Market Size, Report, Trends By 2035," n.d.). Among coumarin subclasses, 4-hydroxycoumarins are of particular pharmaceutical significance, exemplified by warfarin, a first-generation anticoagulant that remains among the 120 most prescribed medications in the United States with over 5 million annual prescriptions (Lin et al., 2013a; Shen et al., 2017).

Industrial coumarin production relies primarily on plant extraction or chemical synthesis. Plant extraction is constrained by low yields, long cultivation times, and seasonal variability (Elmusa and Elmusa, 2024), while the current chemical synthesis routes typically require harsh conditions, toxic reagents, and multiple steps with limited regioselectivity (Citarella et al., 2024; Vargas-Soto et al., 2017). These limitations have motivated the exploration of microbial biosynthesis as a sustainable alternative. Recent studies have demonstrated the biosynthesis of a series of coumarin derivatives in *Escherichia coli* through heterologous expression of salicylate-CoA ligase and the type III polyketide synthase PqsD from *Pseudomonas aeruginosa* (Gan et al., 2025; Lin et al., 2013a, 2013b; Shen et al., 2017).

In this study, we investigated the substrate scope of the PqsD coupled with a promiscuous 6-methylsalicylic acid (6MSA) CoA ligase, MdpB2, for converting substituted salicylic acids into corresponding 4-

hydroxycoumarin derivatives. We found that the MdpB2-PqsD cascade accepted C4- and C5-substituted salicylic acids bearing amino, methyl, and hydroxyl groups, with preference for C5-substituted methyl and amino substrates. As a proof-of-concept for *de novo* pathway construction within this expanded product space, we selected the 6-amino-4-hydroxycoumarin (6A4HC), a pharmaceutically interesting derivative bearing both the characteristic 4-hydroxyl pharmacophore of this subclass and an amino substituent that provides a versatile handle for further derivatization (Ghouse et al., 2023; Jung and Park, 2009; Kasperkiewicz et al., 2020). To access this target biologically, we developed a *de novo* biosynthetic route to its precursor 5-aminosalicylic acid (5ASA), which itself is an FDA-approved anti-inflammatory drug (Segars and Gales, 1992), and coupled it to the MdpB2-PqsD module to achieve the *de novo* microbial production of both 5ASA and 6A4HC. These results highlight the potential of microbial engineering as a sustainable strategy for producing structurally diverse and pharmacologically relevant 4-hydroxycoumarin derivatives.

2. Materials and methods

2.1. DNA Cloning

NEBuilder HiFi assembly mastermix (New England Biolabs) was utilized for plasmid construction via Gibson assembly. Comprehensive information regarding the resulting plasmids is provided in Supplementary Tables S1 and S2. Integrated DNA Technologies supplied all primers used in this study. The PKS genes were first codon-optimized with BaseBuddy (Schmidt et al., 2023) and then synthesized by Genscript. For DNA amplification, PrimeStar GXL mastermix (Takara Bio) was employed, while Zymo Research kits were used for both gel extraction and plasmid isolation.

2.2. Strains and medium

The Guss laboratory at Oak Ridge National Laboratory provided the *Pseudomonas putida* strain AG5577. For all plasmid amplification and molecular cloning procedures, we employed the 5-alpha Iq *E. coli* strain obtained from New England Biolabs. Detailed information on all strains used in this work is provided in Supplementary Table S3. Cultures for plasmid and strain development, as well as seed cultures for fermentation, were grown in LB medium (composed of 10 g/L NaCl, 10 g/L tryptone, and 5 g/L yeast extract). For the production test, the M9YE media was used (M9 minimum media with 5 g/L yeast extract and 20 g/L glucose).

2.3. Strain construction

Strain development involved the use of the SAGE technique for genomic integrations (Elmore et al., 2023). To perform gene deletions, the *pk18sacB* vector system was utilized (Lee et al., 2025). For the creation of in-frame deletions, 1500-bp homologous recombination sequences were selected for both the upstream and downstream flanking regions. Due to the presence of multiple chromosome copies in *P. putida*, target gene elimination was rigorously verified using both negative and positive PCR screenings to ensure a clean genetic background.

2.4. Production Tests

Engineered *P. putida* strains were cultured in M9 minimal medium supplemented with 5 g/L yeast extract and glucose. For substrate-feeding experiments, cultures were supplemented with 20 g/L glucose. For *de novo* production experiments and metabolic engineering efforts, cultures were supplemented with 40 g/L glucose. Production was assessed in 2 mL cultures within 24-well plates, incubated at 30 °C and 200 rpm for 96 hours. Samples were prepared by combining with methanol at a 1:1 ratio (50% methanol) and filtered with the AcroPrep™ Advance 96-well filter plates purchased from Cytiva. The filtrate was then subjected to analysis by liquid chromatography-mass spectrometry (LCMS).

2.5. Product analysis

A reverse-phase C18 column (4.6 x 150 mm, 3.5 µm Agilent) was employed for LCMS. The chromatographic method employed a methanol-water gradient (with 0.1% formic acid) at 0.5 mL/min flow rate: initial 5% methanol (0-1 min), linear increase to 50% (1-4 min), further increase to 95% (4-8 min), hold at 95% (8-10 min), return to 5% (10-16 min), and equilibration (16-18 min). Quantification relied on calibration curves prepared from authentic or commercially available standards.

2.6. Chemical synthesis of 4,6-dihydroxycoumarin and 4,7-dihydroxycoumarin

All reagents were purchased from Sigma-Aldrich and used as received. Reactions were carried out under an atmosphere of nitrogen in flame-dried glassware with magnetic stirring. Flask joints were sealed with rubber septa. ^{1}H NMR and H-decoupled ^{13}C NMR spectra were recorded on Bruker NEO-500 500 MHz spectrometer. Tabulated spectra are reported in ppm using solvent as an internal standard (H-NMR: CD_3OD at 3.21 ppm with trace of HOD at 4.77 ppm; C-NMR: CD_3OD at 49.0 ppm). Data are reported as s = singlet,

d = doublet, t = triplet, q = quartet, sx = sextet, sp=septet, m = multiplet, b = broad; coupling constant(s) in Hz; and integration.

The general procedure for coumarin synthesis was as follows. Dihydroxybenzene (20 mmol) and malonic acid (6.26 g, 60 mmol) were suspended in MTBE (20 mL) and heated to 50°C. The mixture was charged with BF_3-Et_2O (10 mL) dropwise via syringe over 10 min, then the temperature was raised to 80°C. The mixture was refluxed for 24 h. The hot reaction mixture was poured directly into 300 mL of ice water. The precipitate was filtered and washed with MTBE (2 x 10 mL) to afford the product as a solid.

4,7-dihydroxycoumarin:

Following the general procedure using resorcinol (2.20 g, 20 mmol), the product was obtained as an orange solid (0.84 g, 24%). 505 mg of this material was recrystallized in hot water (ca. 50 mL) to afford orange needles (407 mg, 80% recovery).

^{1}H NMR (500 MHz, MeOD) δ 7.73 (d, J = 8.7 Hz, 1H), 6.79 (dd, J = 8.7, 2.3 Hz, 1H), 6.69 (d, J = 2.3 Hz, 1H). ^{13}C NMR (126 MHz, MeOD) δ 167.7, 165.6, 162.3, 155.8, 124.5, 112.7, 108.0, 101.7. Alpha CH proton signal is not present due to rapid tautomerization and proton exchange.

4,6-dihydroxycoumarin:

Following the general procedure using p-hydroquinone (2.20 g, 20 mmol), the product was obtained as a faintly pink solid (0.76 g, 21%).

^{1}H NMR (500 MHz, MeOD) δ 7.23 (d, J = 2.9 Hz, 1H), 7.19 (d, J = 8.9 Hz, 1H), 7.08 (dd, J = 8.9, 2.9 Hz, 1H). ^{13}C NMR (126 MHz, MeOD) δ 166.9, 165.2, 153.9, 147.3, 120.7, 117.2, 116.4, 107.2. Alpha CH proton signal is not present due to rapid tautomerization and proton exchange.

3. Results

3.1. Characterizing the substrate scope of the MdpB2-PqsD cascade

Previous studies have shown that PqsD from *Pseudomonas aeruginosa* natively accepts unsubstituted salicyloyl-CoA (Lin et al., 2013a), but its tolerance toward substituted analogs remains relatively uncharacterized. Gan et al. reported that PqsD accepts 2,5-dihydroxybenzoate in addition to salicylic acid (Gan et al., 2025). However, we suspected that this substrate restriction was likely due to the limited substrate scope of SdgA, which is the CoA ligase reported to specifically activate salicylic acid to its CoA thioesters. To address this hypothesis, we selected an alternative CoA ligase, MdpB2, from the

Maduropeptin biosynthetic cluster (Van Lanen et al., 2007). MdpB2 is known to catalyze CoA activation of 6-methylsalicylic acid, a substituted analog of salicylic acid, suggesting that it may possess broader substrate flexibility than SdgA. Both SdgA-PqsD and MdpB2-PqsD pathways were integrated into *P. putida* AG5577 (Schmidt et al., 2023), creating strains PP-SdgA-PqsD and PP-MdpB2-PqsD, respectively. Unexpectedly, expression of the SdgA-PqsD pathway resulted in severe growth defects in *P. putida*, so subsequent studies focused solely on the MdpB2-PqsD pathway.

Next, we investigated the substrate scope of the MdpB2-PqsD pathway. A panel of salicylic acid derivatives containing $–NH_2$, $–NO_2$, $–CH_3$, –OMe, or –OH substituents at positions C3, C4, C5, or C6 was supplied (**Fig. 1a**). LCMS analysis of the resulting cultures revealed that $–NH_2$, $–CH_3$, and –OH substituents at the C4 (*para*) or C5 (*meta*) positions were successfully incorporated, yielding their corresponding coumarin derivatives (**Fig. 1**). In contrast, no products were detected for the C3/C6 isomers or the $–NO_2$/–OMe substituted substrates. For methyl and amino substrates, the cascade pathway in *P. putida* showed a clear positional preference for C5 (meta) substrates, evidenced by the significantly higher production titers of the 6-substituted coumarin (derived from 5-substituted salicylic acid) compared to the 7-substituted coumarin (derived from 4-substituted salicylic acid) (**Fig. 1d, e**). Nonetheless, this positional preference was not observed for hydroxy-substituted substrates, as 5-hydroxysalicylic acid and 4-hydroxysalicylic acid produced comparable titers of 4,6-dihydroxycoumarin (4,6DHC) and 4,7-dihydroxycoumarin (4,7DHC), respectively (**Fig. 1d, e**). These findings greatly expanded the biosynthetic repertoire for coumarin production, especially for $–NH_2$ and –OH substituents that often exhibit unique biological activities.

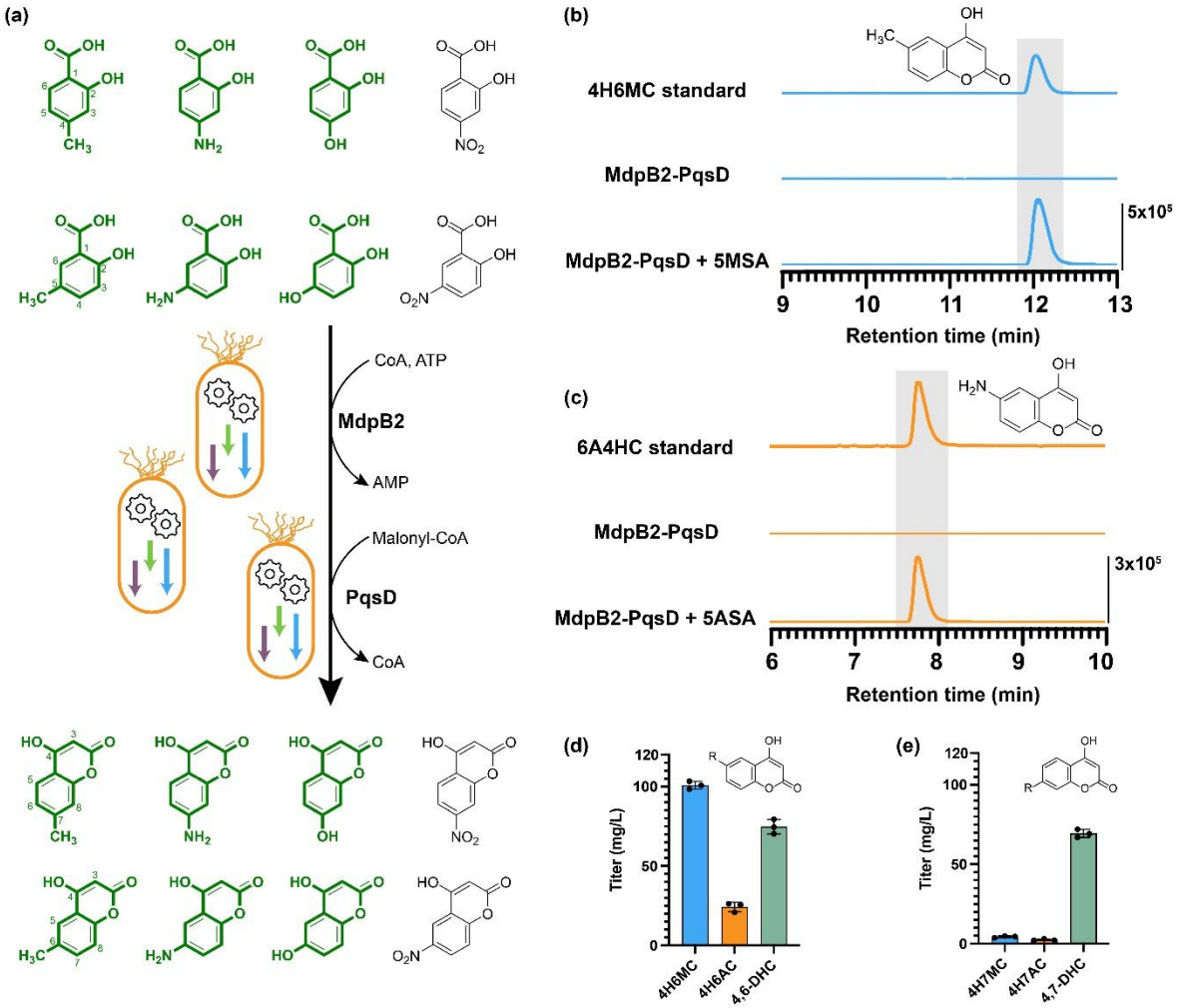


Figure 1. Substrate scope of the MdpB2-PqsD cascade for the biosynthesis of substituted coumarins. **(a)** Schematic of the MdpB2-PqsD pathway and the salicylic acid derivatives tested. Accepted substrates and resulting products are shown in green. Unaccepted substrates and expected products are shown in grey. **(b)** Representative LCMS analysis showing production of 4-hydroxy-6-methylcoumarin (4H6MC) from 5MSA by strain PP-MdpB2-PqsD. **(c)** Representative LCMS analysis showing production of 6A4HC from 5ASA by MdpB2-PqsD. **(d)** Titer of 4H6MC and 6A4HC derived from C5-substituted salicylic acids. **(e)** Titer of 4H7MC and 7A4HC derived from C4-substituted salicylic acids. The MdpB2-PqsD pathway produced higher titers from C5-substituted substrates than from the corresponding C4-substituted substrates for methyl and amino analogs, but not for hydroxy analogs. Error bars represent standard deviations from three independent biological replicates.

3.2. *De novo* biosynthesis of 5ASA

As a proof-of-concept for *de novo* pathway construction within the expanded product space enabled by the MdpB2-PqsD module, we selected 6A4HC as the demonstration target, because it may exhibit promising pharmacological properties (anti-inflammatory, antioxidant, and anticoagulant) attributed to the synergistic effect of the 4-hydroxy and 6-amino substituents (Abazari et al., 2025; Jung and Park, 2009; Saadati et al., 2024). Moreover, its precursor 5-aminosalicylic acid (5ASA), as demonstrated in the previous studies, is an FDA-approved anti-inflammatory drug (Segars and Gales, 1992) used to treat ulcerative colitis and Crohn's disease, with annual sales exceeding $1 billion globally, yet no biosynthetic route to 5ASA has been established to date.

To develop a *de novo* biosynthetic pathway for 5ASA in *P. putida*, we first exploited the inherent flexibility of established microbial pathways that generate salicylic acid analogs. Given that these enzymes naturally process structurally similar compounds, we anticipated they might demonstrate substrate promiscuity toward various aminobenzoate precursors. Rather than pursuing a route in which an amino group would be installed directly onto a hydroxylated benzoic acid scaffold, we focused on identifying enzymes capable of hydroxylating an aminobenzoate intermediate, because aromatic hydroxylation is a well-precedented transformation in microbial metabolism (Gan et al., 2025; Ullrich and Hofrichter, 2007), whereas amination of a salicylic acid-like substrate is less common and not well characterized. We therefore selected several candidate hydroxylation systems based on their reported native activities. CreL, a flavin-dependent monooxygenase from the cremeomycin biosynthetic pathway, is involved in the hydroxylation of the 3-amino-4-hydroxybenzoic acid (3,4AHBA) to the 3-amino-2,4-dihydroxybenzoate (3,2,4ADBA) (Waldman et al., 2015) (**Fig 2a**). We also tested PtmB3, a flavin-dependent benzoate hydroxylase from the platensimycin biosynthetic pathway which has a similar function as the CreL (Smanski et al., 2011) (**Fig. 2a**). For both CreL and PtmB3, we hypothesized that even though their native substrates require a hydroxyl substituent at the para position, replacement of that hydroxyl group with an amino group might still be tolerated, allowing ortho-hydroxylation of 3-aminobenzoic acid (3ABA) to form 5ASA or 3-aminosalicylic acid (3ASA). The second target we pursued was the PhgACB system, consisting of a CoA ligase PhgC, a CoA-dependent hydroxylase PhgA, and a thioesterase PhgB (Zhao et al., 2018). The PhgACB enzyme cascade converts 4-hydroxybenzoate (4HBA) to gentisate (2,5-dihydroxybenzoic acid, 2,5DHBA) (**Fig 2a**). In this case, we hypothesized that CoA-mediated activation might broaden substrate tolerance and enable the pathway to accept 4ABA while still directing hydroxylation at the *ortho* position. The last target enzyme we selected was the 3-hydroxybenzoate 6-hydroxylase (3HB6H), which is a flavin-dependent monooxygenase that naturally converts 3-hydroxybenzoic acid (3HBA) into 2,5DHBA (Montersino et al., 2013; Montersino and van Berkel, 2012) (**Fig 2a**). Because 3ABA closely resembles the native substrate 3HBA, differing only by replacement of the hydroxyl group with an amino group, we hypothesized that 3HB6H might catalyze ortho-hydroxylation of 3ABA to yield 5ASA.

We first confirmed the *in vivo* activity of the candidate enzymes using their native substrates. Interestingly, even in the absence of an exogenous supply of 3HBA or 4HBA, the strains PP-PhgACB and PP-3HB6H still produced detectable 2,5DHBA, suggesting that *P. putida* may natively synthesize a small amount of relevant aromatic precursors **(Supplementary Fig. S1)**. When 3HBA or 4HBA was supplemented to the corresponding pathway, 2,5DHBA titers increased substantially, confirming that the introduced pathway enzymes were active *in vivo* **(Fig 2b; Supplementary Fig. S1)**.

We then tested these candidates by supplying the predicted aminobenzoate substrates in cultures of *P. putida* strains PP-CreL, PP-PtmB3, PP-PhgACB, PP-3HB6H. PP-CreL, PP-PtmB3, and PP-3HB6H were evaluated using 3ABA, whereas PP-PhgACB was tested using 4ABA. Under the conditions examined, we failed to observe detectable 5ASA in strains with CreL, PtmB3, or PhgACB. In contrast, strains expressing 3HB6H (PP-3HB6H) supplemented with 3ABA in the medium resulted in the formation of 5ASA **(Fig 2b)**. Quantitative analysis revealed that when PP-3HB6H were supplied with 200 mg/L 3HBA, the production of 2,5DHBA reached 108.6 mg/L, while supplementation with 200 mg/L 3ABA yielded 125.1 mg/L 5ASA (**Fig 2c**). Given the successful bioconversion of 3ABA to 5ASA, we next sought to construct an upstream pathway for *de novo* 3ABA biosynthesis from cellular metabolism.

Using 3-dehydroshikimate (3DHS) as the branch point, we engineered a pathway that shunts this native shikimate-pathway intermediate of *P. putida* into 3ABA biosynthesis. For conversion of 3DHS to 3ABA, we selected PctV, a pyridoxal 5'-phosphate (PLP)-dependent aminotransferase from *Streptomyces pactum*, which catalyzes the transamination of 3DHS using L-glutamate as the amino donor (Hirayama et al., 2013). A codon-optimized *pctV* gene was synthesized for expression in *P. putida* and integrated into BL3 site under control of P_{LLacO1} promoter, and the resulting strain, PP-pctV, produced 0.64 mg/L 3ABA from glucose, confirming that PctV can establish a *de novo* pathway to 3ABA in this host **(Fig 2d)**. Together with 3HB6H, this two-step route — transamination of 3DHS to 3ABA followed by hydroxylation to 5ASA **(Fig 2e)** — constitutes a complete *de novo* biosynthetic pathway from central metabolism to 5ASA. Although the initial 3ABA titer was low, this result is consistent with previous reports that *de novo* microbial production of 3ABA remains challenging (Zhang and Stephanopoulos, 2016), likely due to the limited activity of 3ABA synthases (Hirayama et al., 2015, 2013). Notably, the achieved titer is comparable to the highest 3ABA production reported from a single microbial strain (Zhang and Stephanopoulos, 2016), demonstrating the feasibility of this pathway in *P. putida*.

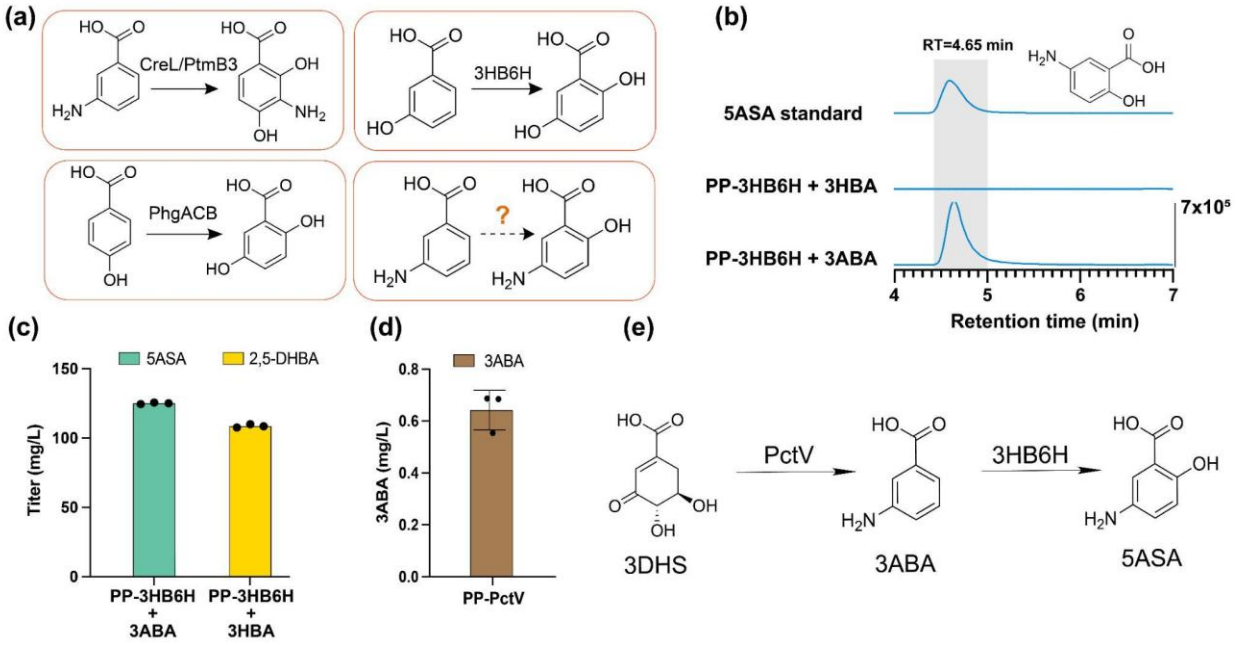


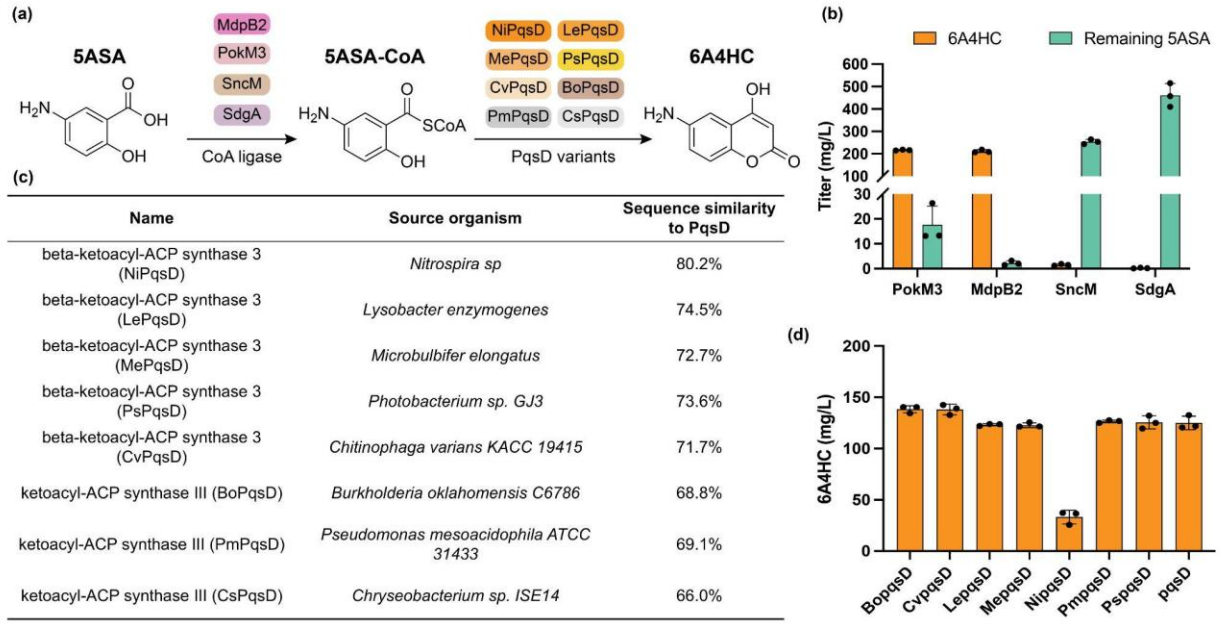
Figure 2. Identification of a *de novo* route to 5ASA. (a) Candidate enzyme systems evaluated for aromatic hydroxylation of aminobenzoate-related substrates. CreL/PtmB3, PhgACB, and 3HB6H were tested based on their hypothesized substrate promiscuity toward 3ABA. **(b)** LC–MS analysis showing the production of 5ASA by strain PP-3HB6H when 3ABA was supplied as the precursor. The trace shown corresponds to m/z = 154 ($[M+H]^+$, ESI mode). **(c)** Production of 5ASA from 3ABA and 2,5DHB from 3HBA by strain PP-3HB6H after feeding 200 mg/L substrate. **(d)** *De novo* 3ABA accumulation in strain PP-PctV. **(e)** Biosynthetic pathway from the shikimate pathway intermediate 3DHS to 5ASA through sequence conversion by PctV and 3HB6H. Error bars represent standard deviations from three independent biological replicates.

3.3 Optimizing the biosynthesis efficiency of 6A4HC through enzyme screening

With the successful establishment of *de novo* 3ABA biosynthesis, we next sought to optimize the pathway to produce 6A4HC before combining it with the 3ABA producing strain. The conversion of 5ASA to 6A4HC requires a CoA ligase to activate it **(Fig 3a)**. Thus, we sought to identify an optimal enzyme combination for the most efficient conversion. We first screened a series of CoA ligases, including MdpB2, a 6-methylsalicylic acid-AMP ligase from *Actinomadura madurae* (Ling et al., 2010); PokM3, a functionally similar 6-methylsalicylic acid-AMP ligase from *Streptomyces diastatochromogenes* (Guo et al., 2018); SncM, a putative 5-aminosalicylic acid-AMP ligase identified through bioinformatics analysis (Ma et al., 2025); and the previously mentioned SdgA, the salicylic acid-AMP ligase from *Streptomyces sp.* strain WA 46 (Gan et al., 2025; Lin et al., 2013a) (**Fig. 3a**).

Feeding experiments were conducted by co-expressing each candidate enzyme with PqsD and measuring the resulting 6A4HC titers upon feeding 500 mg/L of 5ASA **(Fig 3b)**. SdgA, which had been previously demonstrated to convert salicylic acid to 4-hydroxycoumarin when paired with PqsD in *E. coli* (Lin et al., 2013a), caused severe growth inhibition when expressed in *P. putida*, suggesting host incompatibility issues. Consequently, 6A4HC production in the strain PP-SdgA-PqsD was negligible, with the majority of fed 5ASA (460.6 mg/L) remaining unconverted. Strain PP-SncM-PqsD yielded only trace amounts of 6A4HC (1.6 mg/L), despite bioinformatics predictions suggesting potential activity toward this aminosalicylate substrate (Ma et al., 2025). In contrast, both strains PP-PokM3-PqsD and PP-MdpB2-PqsD demonstrated substantial activity toward 5ASA. Strains expressing PokM3 consumed 96.5% of fed 5ASA, producing 216.4 mg/L of 6A4HC with 17.6 mg/L of 5ASA remaining unconverted, corresponding to a 37.4% molar yield relative to the initial 500 mg/L feed. Comparatively, the MdpB2 group achieved near-complete 5ASA depletion (99.6% consumption), yielding 211.4 mg/L of 6A4HC, which represents a 36.5% molar yield. While the 6A4HC titers are comparable between PokM3- (216.38 mg/L) and MdpB2-based (211.38 mg/L) pathways, the stronger and more consistent 5ASA consumption observed with MdpB2 suggests that it drives flux with more robustness. Based on these results, MdpB2 was selected as the preferred CoA ligase for subsequent pathway assembly and optimization.

Having identified MdpB2 as the optimal CoA ligase, we next investigated whether alternative type III PKS variants might offer improved catalytic efficiency for the condensation and cyclization step. We identified seven PqsD homologs through BLAST analysis based on high amino acid sequence similarity (**Fig 3a, c**). These homologs, designated BoPqsD, CvPqsD, CsPqsD, LePqsD, MePqsD, NiPqsD, PmPqSD, and PsPqsD, were individually paired with MdpB2 under the control of P_{LLacO1} promoter and integrated into *P. putida* at the Bxb1 site to evaluate for 6A4HC production. All integrations were successful, creating the strains PP-MdpB2-BoPqsD, PP-MdpB2-CvPqsD, PP-MdpB2-LePqsD, PP-MdpB2-MePqsD, PP-MdpB2-NiPqsD, PP-MdpB2-PmPqsD, and PP-MdpB2-PsPqsD, respectively, except for CsPqsD. Integration of the *CspqsD* gene with the *mdpB2* resulted in severe growth defects, making it difficult to obtain positive clones. When the strains harboring different PqsD variants were supplemented with 200 mg/L 5ASA, six of the seven homologs produced comparable amounts of 6A4HC, ranging from 123.2 to 138.4 mg/L, whereas NiPqsD exhibited markedly reduced activity, producing only 33.2 mg/L of 6A4HC **(Fig 3d)**. Our results now experimentally validated these putative enzymes which were previously only annotated as putative type III PKSs. These variants are capable of catalyzing 6H4AC formation *in vivo* and likely have a similar function as the PqsD from *P. aeruginosa*. Given that the original PqsD has been extensively characterized and validated for 4-hydroxycoumarin biosynthesis, we selected PqsD as the preferred PKS in the subsequent experiments.



(c)

Name	Source organism	Sequence similarity to PqsD
beta-ketoacyl-ACP synthase 3 (NiPqsD)	*Nitrospira sp*	80.2%
beta-ketoacyl-ACP synthase 3 (LePqsD)	*Lysobacter enzymogenes*	74.5%
beta-ketoacyl-ACP synthase 3 (MePqsD)	*Microbulbifer elongatus*	72.7%
beta-ketoacyl-ACP synthase 3 (PsPqsD)	*Photobacterium sp. GJ3*	73.6%
beta-ketoacyl-ACP synthase 3 (CvPqsD)	*Chitinophaga varians KACC 19415*	71.7%
ketoacyl-ACP synthase III (BoPqsD)	*Burkholderia oklahomensis C6786*	68.8%
ketoacyl-ACP synthase III (PmPqsD)	*Pseudomonas mesoacidophila ATCC 31433*	69.1%
ketoacyl-ACP synthase III (CsPqsD)	*Chryseobacterium sp. ISE14*	66.0%

Figure 3. Screening of CoA ligases and PqsD homologs for 6A4HC production from 5ASA. (a) Biosynthetic conversion of 5ASA to 6A4HC through CoA ligase-mediated activation followed by PqsD-catalyzed cyclization. **(b)** Comparison of candidate CoA ligases co-expressed with PqsD. **(c)** Seven PqsD homologs were selected by BLAST analysis based on amino acid sequence similarity to PqsD. **(d)** Evaluation of seven PqsD homologs paired with MdpB2 using 200 mg/L 5ASA. Six homologs produced comparable 6A4HC titers, whereas NiPqsD showed substantially lower activity. Error bars represent standard deviations from three independent biological replicates.

3.4 Metabolic engineering for *de novo* coumarin production

Based on the enzyme screening results, we assembled the complete *de novo* biosynthetic pathway for 6A4HC by combining the upstream 5ASA pathway (PctV and 3HB6H) with the downstream coumarin-forming module (MdpB2 and PqsD), creating strain PP-CZ0 **(Fig 4a)**. Surprisingly, the strain PP-CZ0 did not produce detectable 6A4HC **(Fig 4b)**, which was likely due to the low production titer of 3ABA from PctV (**Fig. 2d**). Besides the low activity of the PctV(Hirayama et al., 2015; Zhang and Stephanopoulos, 2016), this limitation likely also arose from two related features of native *P. putida* metabolism. First, 3DHS biosynthesis depends on the carbon flux in the shikimate pathway from phosphoenolpyruvate (PEP) and erythrose-4-phosphate (E4P), yet PEP is simultaneously consumed by central metabolic reactions such as pyruvate kinase and PEP carboxylase (Koendjbiharie et al., 2021; Li et al., 2022; Yu et al., 2016). Second, 3DHS itself is a metabolic branch-point intermediate that can be consumed by endogenous enzymes and therefore may not accumulate to levels sufficient to drive the heterologous PctV reaction.

To overcome these limitations, we redirected the metabolic flux in the central carbon metabolism to improve precursor delivery into 3DHS while minimizing competing sinks. First, we targeted two major PEP-consuming reactions: PykA, which converts PEP irreversibly to pyruvate (Schormann et al., 2019), and Ppc, which channels PEP to oxaloacetate (Kai et al., 1999). Disrupting these reactions was expected to reduce PEP loss to lower metabolism and preserve carbon for DAHP formation. To further strengthen flux from DAHP toward 3DHS, we simultaneously introduced additional copies of aroQ, which catalyzes the direct conversion of 3-dehydroquinate to 3DHS. AroQ-I and aroQ-II were inserted at the *ppc* and *pykA* loci, respectively. Second, we replaced HexR with a feedback-resistant *aroG** allele. HexR is a global repressor of upper glucose catabolism in *P. putida* (Bentley et al., 2020; del Castillo et al., 2008; Elmore et al., 2020); its removal is known to activate genes involved in glucose catabolism and augment the availability of 3PGP and PEP (Dvořák et al., 2024). Third, because the *phaABC2* gene cluster will divert surplus carbon into polyhydroxyalkanoate (PHA) for storage (Manoli et al., 2022), we deleted the *phaABC2* cluster to limit diversion of carbon into PHA storage. In *P. putida*, *benA* and *benB* divert benzoate-like aromatic intermediates into catechol (Incha et al., 2020). Because 3ABA and 5ASA are both aromatic compounds, *benAB* was also deleted to prevent the cell from potentially catabolizing these benzoate derivatives.

The resulting strain, designated PP-CZ1 (Δ*benAB* Δ*ppc::aroQ-I* Δ*pykA::aroQ-II* Δ*hexR::*PLlacO1-*aroG_fbr* Δ*PhaABC2* BL3*::pctV*), exhibited a 13-fold increase in 3ABA accumulation relative to the parental strain (CZ0), with titers increasing from 0.64 mg/L to 4.65 mg/L **(Fig 4b)**. To further improve the 3ABA titer, we deleted *gcd* in strain PP-CZ1 to form strain PP-CZ2. The *gcd* gene encodes the periplasmic glucose dehydrogenase that oxidizes glucose to gluconate (An and Moe, 2016). Because wild-type *P. putida* directs most glucose through this oxidative route (Nikel et al., 2015), removing *gcd* was expected to force a larger fraction of glucose into cytoplasmic phosphorylation and central carbon metabolism and thereby improve precursor supply for aromatic biosynthesis. Interestingly, deleting *gcd* (PP-CZ2) resulted in a statistically insignificant increase in 3ABA production **(Fig 4b)**, which may indicate the carbon supply is no longer an issue for over producing the 3ABA.

For the production of 3ABA, PctV also requires pyridoxal 5′-phosphate (PLP) as an essential cofactor for the enzymatic reaction (Hirayama et al., 2013). We hypothesized that PLP availability might be the limiting factor under elevated pathway flux, thereby constraining further improvements in 3ABA production. Therefore, we introduced *pdxST* from *Bacillus subtilis 168,* a PLP biosynthetic module, into strain CZ2 (Wang et al., 2020). The resulting strain, PP-CZ3, produced 7.5 mg/L 3ABA, representing a 21-fold improvement over the parental strain and a 1.7-fold increase relative to the CZ2 strain **(Fig 4b)**. This finding demonstrated that cofactor supply imposed an additional constraint on pathway performance.

During the cultivation of strain PP-CZ3, we observed a pronounced brown coloration **(Supplementary Fig. S2, Fig 4b-d)**. Browning can arise when phenolic or catechol-like compounds are oxidized to quinones and then undergo further non-enzymatic reactions that generate brown pigments (Tilley et al., 2023). Given that protocatechuate possesses a catechol structure and is therefore susceptible to oxidation, we hypothesized that the enhanced carbon flux toward 3DHS was being redirected by QuiC in *P. putida* to protocatechuate (Dal et al., 2005), thereby contributing to pigment formation. In addition to QuiC, AroE catalyzes 3DHS to shikimate (Anton and Coggins, 1988; Chaudhuri and Coggins, 1985; Dansette and Azerad, 1974), the precursor for aromatic amino acid biosynthesis. Both reactions compete with PctV for 3DHS. To evaluate the individual contributions of these competing branch points, we constructed strains harboring deletions of *aroE* and *quiC* independently. Interestingly, *aroE* knockout resulted in significant growth inhibition and thus made it difficult to obtain a positive clone, possibly due to the essentiality of aromatic amino acid production through the shikimate biosynthesis. In contrast, the *quiC* knockout was tolerated. The deletion of *quiC* significantly reduced the formation of the brown pigment (**Supplementary Fig. S2)**. We subsequently integrated the 3HB6H and MdpB2-PqsD to generate strain PP-CZ4. The strain PP-CZ4 produced 5.64 mg/L 6A4HC with less than 2 mg/L 3ABA remaining in the culture **(Fig 4b-d)**, which represented a productivity of 0.0588 mg/L/h and a yield of 0.141 mg/g glucose. These results indicate that blocking protocatechuate formation effectively redirects carbon flux toward 6A4HC biosynthesis. Consequently, we successfully established the *de novo* biosynthesis of 6A4HC. To determine product localization, we analyzed the culture supernatant and the cell pellet separately, revealing that 6A4HC predominantly accumulates in the extracellular medium with only trace amounts retained intracellularly (**Supplementary Fig. S3**)

To further enhance the titer of 6A4HC, we introduced an additional genomic copy of *pctV* into strain PP-CZ4, generating strain PP-CZ5. We suspected the turnover rate of the PctV may be slow as both carbon flux and cofactor supply have been boosted. While the strain PP-CZ5 enabled a slightly increased 6A4HC titer at 7.56 mg/L (0.079 mg/L/h productivity and 0.189 mg/g glucose yield) **(Fig 4d)**, the difference was not statistically significant, indicating that increasing *pctV* copy number was insufficient to substantially improve pathway output; future metabolic engineering including enzyme engineering and host engineering are required to further push the titer.

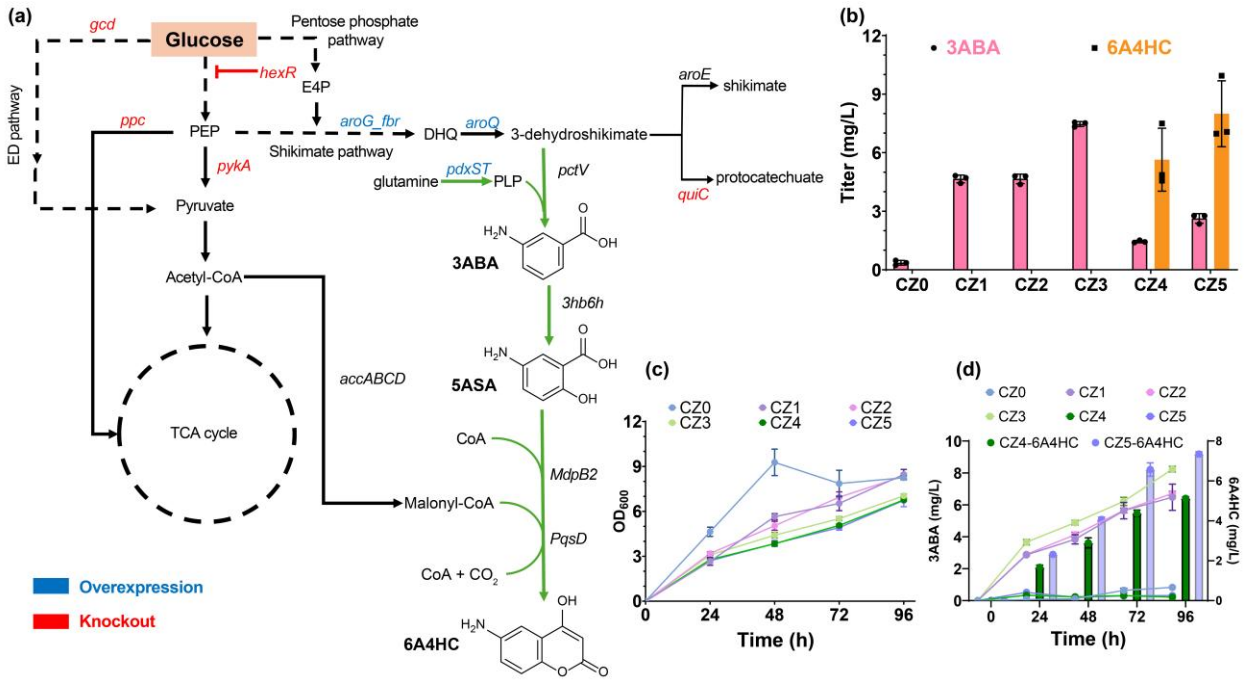


Figure 4. Metabolic engineering of *P. putida* for *de novo* 6A4HC biosynthesis. (a) Engineered pathway from glucose to 6A4HC with overexpression (blue) and knockout (red) targets indicated. **(b)** Accumulation of 3ABA and 6A4HC across the sequentially engineered strains PP-CZ0 to PP-CZ5. For PP-CZ4 and PP-CZ5, the 3ABA titer represents the amount remaining after conversion to 6A4HC. 6A4HC was detected only in strains PP-CZ4 and PP-CZ5. **(c)** Growth curve for strains PP-CZ0 to PP-CZ5. **(d)** Time-course accumulation of 3ABA and 6A4HC for strain PP-CZ0 to PP-CZ5. Error bars represent standard deviations from three independent biological replicates.

4. Discussion and conclusions

This study demonstrated a *de novo* microbial biosynthesis pathway for an amino-substituted 4-hydroxycoumarin and the identification of a previously uncharacterized enzyme activity that provides the first biological route to 5ASA. Together, these findings expand both the enzymatic toolkit and the design logic available for future coumarin pathway engineering. As demand grows for sustainable production of complex aromatic pharmaceuticals, the modular biosynthetic platform described here provides a validated foundation from which the broader family of substituted 4-hydroxycoumarin derivatives can be systematically pursued.

Several limitations of this study warrant consideration. Most notably, the final *de novo* 6A4HC titer of 7.56 mg/L remains low and far from industrial relevance. To quantify this gap, we conducted a basic techno-economic analysis. Because the chemical synthesis of the functionalized 6A4HC requires more complex

steps, we conservatively benchmarked our target against the bulk commercial price of the structurally related 4-hydroxycoumarin (~$228/kg). To achieve a highly competitive minimum selling price (MSP) of $228/kg, the *de novo* biosynthesis would require a target titer to be higher than 370 mg/L. To contextualize the metabolic feasibility of reaching these industrial targets, the absolute theoretical maximum yield of 6A4HC based on carbon stoichiometry is 0.655 g/g glucose, which corresponds to approximately 26.2 g/L under our cultivation conditions. While our current titer represents ~0.03% of this absolute ceiling, such yields are typical for proof-of-concept *de novo* platforms prior to extensive optimization. While rational host engineering substantially improved pathway performance, as evidenced by the 21-fold increase in 3ABA accumulation, the absolute 3ABA titers remained modest, suggesting that flux into this pathway is still insufficient. This limitation likely stems from fundamental biological constraints and two related bottlenecks. First, 3DHS is a native branch-point intermediate that is consumed by competing pathways, including one major pathway to shikimate catalyzed by AroE, whose knockout significantly compromises cell growth. Second, PctV represents a remaining pathway bottleneck, as demonstrated in other studies (Hirayama et al., 2015, 2013; Zhang and Stephanopoulos, 2016). As a heterologous PLP-dependent aminotransferase, its activity in *P. putida* may be constrained. Furthermore, the maximum theoretical carbon limit assumes a frictionless metabolic network and does not account for host energy metabolism. *P. putida* relies natively on the Entner-Doudoroff (ED) pathway, which generates less ATP per glucose molecule compared to the traditional Embden-Meyerhof-Parnas (EMP) pathway. This structural energy deficit naturally restricts the achievable biological ceiling for our highly ATP- and NADPH-intensive cascade. Further optimization can focus on increasing effective 3DHS availability without impairing host growth, screening effective PctV homologs, and potential protein engineering to improve the efficiency of the aminotransferase step. To realize this, emerging AI-guided protein engineering tools (e.g., EvolvePro and AlphaFold) offer powerful predictive capabilities to rationally navigate the fitness landscape of enzymes like PctV (Abramson et al., 2024; Jiang et al., 2025; Singh et al., 2025). Because the downstream promiscuous module (3HB6H and MdpB2-PqsD) already exhibits robust conversion efficiency, improving upstream 3ABA supply is the most critical target for titer improvement. Coupling these computational AI designs with the development of genetically encoded biosensors will be instrumental in establishing high-throughput screening platforms. This synergistic strategy will enable the rapid identification of high-producing PctV variants, thereby relieving this carbon choke point and maximizing the efficiency of the *de novo* production platform.

Despite these current limitations, this study establishes a foundational framework with significant long-term implications that should not be understated. The achievement of *de novo* 6A4HC biosynthesis from glucose, even though modest in titer, represents a conceptual breakthrough, as no microbial route to this compound or its direct precursor 5ASA had previously been reported. The discovery that 3hb6h exhibits

promiscuous activity toward 3ABA is itself a significant enzymological finding that opens an entirely new enzymatic route to 5ASA (mesalamine), an FDA-approved anti-inflammatory drug used primarily for the treatment of ulcerative colitis (Segars and Gales, 1992). Commercially, the mesalamine product Lialda has achieved sales of almost US $1 billion per year in the United States. A microbial platform for *de novo* 5ASA biosynthesis would therefore be valuable both as an intermediate for 6A4HC production and as an alternative route to this important pharmaceutical. The 4-hydroxycoumarin scaffold of 6A4HC is widely recognized for its pharmacological relevance, with derivatives exhibiting diverse biological activities, including anticoagulant, anti-inflammatory, antimicrobial, antiviral, and anticancer effects(Raj and Lee, 2020; Sadan et al., 2025; Vlachou et al., 2022). Although the biological activity of 6A4HC itself remains to be established, the pharmacological relevance of the 4-hydroxycoumarin scaffold provides a rationale for future investigation of the bioactivity and therapeutic potential of 6A4HC. The broad substrate scope demonstrated for the MdpB2-PqsD module, successfully accommodating $–NH_2$, $–CH_3$, and –OH substituents at multiple positions, further suggests that this platform could serve as a generalizable chassis for producing a diverse library of pharmacologically relevant 4-hydroxycoumarin derivatives beyond 6A4HC alone. In addition, we also experimentally characterized seven putative PqsD-like enzymes and confirmed their *in vivo* activities in forming the 4-hydroxycoumarin derivative 6A4HC. Taken together, this work lays the groundwork upon which future engineering cycles can build, positioning microbial biosynthesis as a promising sustainable alternative to chemical synthesis routes that currently depend on hazardous reagents and multi-step processes (Citarella et al., 2024; Vargas-Soto et al., 2017).

Acknowledgement

This work was carried out at the US Department of Energy (DOE) Joint BioEnergy Institute (https://www.jbei.org/) supported by the DOE, Office of Science, Office of Biological and Environmental Research through contract number DE-AC02-05CH11231 between Lawrence Berkeley National Laboratory and the DOE, and the DOE Distinguished Scientist Fellow Program to J.D.K. We also acknowledge support from the Defense Advanced Research Projects Agency (DARPA) under BFS Fund 28761 (Sponsor Award No. HR0011-25-9-0061). We also thank the help from Dr. Chang Dou at Advanced BioProcess Development Unit (ABPDU), Lawrence Berkeley National Laboratory for helpful discussion about the basic techno-economic analysis.

Competing interest

J.D.K. has financial interests in Ansa Biotechnologies, Apertor Pharma, Berkeley Yeast, BioMia, Cyklos Materials, Demetrix, Lygos, Napigen, ResVita Bio, QSX Bio, and Zero Acre Farms. The other authors declare no competing interests. Aspects of this work are or will be patent pending, filed, or to be filed by The Regents of the University of California. C.Z., N.C., D.H., C.L., and J.D.K. are the listed inventors.

Author Contribution:

C.Z. and C.L. conceived the main idea of the project. C.Z. conducted the majority of the experiments. J.H., D.H., and N.C., participated in the project. C.V. synthesized the coumarin standards for the project. Y.L. conducted the basic techno-economic analysis. C.Z. and C.L. drafted the manuscript. J.D.K. and C.L. supervised the study and revised the manuscript.

References

Abazari, A., Sarrafi, Y., Taheri, P., Tajbakhsh, M., 2025. Synthesis, biological evaluation, and molecular docking of novel coumarin-based bisimine derivatives. Sci. Rep. 15, 42366.

Abramson, J., Adler, J., Dunger, J., Evans, R., Green, T., Pritzel, A., Ronneberger, O., Willmore, L., Ballard, A.J., Bambrick, J., Bodenstein, S.W., Evans, D.A., Hung, C.-C., O'Neill, M., Reiman, D., Tunyasuvunakool, K., Wu, Z., Žemgulytė, A., Arvaniti, E., Beattie, C., Bertolli, O., Bridgland, A., Cherepanov, A., Congreve, M., Cowen-Rivers, A.I., Cowie, A., Figurnov, M., Fuchs, F.B., Gladman, H., Jain, R., Khan, Y.A., Low, C.M.R., Perlin, K., Potapenko, A., Savy, P., Singh, S., Stecula, A., Thillaisundaram, A., Tong, C., Yakneen, S., Zhong, E.D., Zielinski, M., Žídek, A., Bapst, V., Kohli, P., Jaderberg, M., Hassabis, D., Jumper, J.M., 2024. Accurate structure prediction of biomolecular interactions with AlphaFold 3. Nature 630, 493–500.

Al-Warhi, T., Sabt, A., Elkaeed, E.B., Eldehna, W.M., 2020. Recent advancements of coumarin-based anticancer agents: An up-to-date review. Bioorg. Chem. 103, 104163.

Annunziata, F., Pinna, C., Dallavalle, S., Tamborini, L., Pinto, A., 2020. An overview of coumarin as a versatile and readily accessible scaffold with broad-ranging biological activities. Int. J. Mol. Sci. 21, E4618.

Anton, I.A., Coggins, J.R., 1988. Sequencing and overexpression of the Escherichia coli aroE gene encoding shikimate dehydrogenase. Biochem. J. 249, 319–326.

Balewski, Ł., Szulta, S., Jalińska, A., Kornicka, A., 2021. A mini-review: Recent advances in coumarin-metal complexes with biological properties. Front. Chem. 9, 781779.

Bentley, G.J., Narayanan, N., Jha, R.K., Salvachúa, D., Elmore, J.R., Peabody, G.L., Black, B.A.,

Ramirez, K., De Capite, A., Michener, W.E., Werner, A.Z., Klingeman, D.M., Schindel, H.S., Nelson, R., Foust, L., Guss, A.M., Dale, T., Johnson, C.W., Beckham, G.T., 2020. Engineering glucose metabolism for enhanced muconic acid production in Pseudomonas putida KT2440. Metab. Eng. 59, 64–75.

Chaudhuri, S., Coggins, J.R., 1985. The purification of shikimate dehydrogenase from Escherichia coli. Biochem. J. 226, 217–223.

Citarella, A., Vittorio, S., Dank, C., Ielo, L., 2024. Syntheses, reactivity, and biological applications of coumarins. Front. Chem. 12, 1362992.

Cocco, A., Caria, P., Sanna, G., Stagi, L., Cadoni, E., Corpino, R., Ricci, P.C., Carbonaro, C.M., Secci, F., 2021. Synthesis and photophysical properties of fluorescent 6-aryl-D-π-A coumarin derivatives. ACS Omega 6, 33708–33716.

Coumarin and its derivatives, 2021. . Mdpi AG.

Coumarin Market Size, Report, Trends By 2035 [WWW Document], n.d. URL https://www.marketreportsworld.com/market-reports/coumarin-market-14715247 (accessed 6.3.26).

Dal, S., Trautwein, G., Gerischer, U., 2005. Transcriptional organization of genes for protocatechuate and quinate degradation from Acinetobacter sp. strain ADP1. Appl. Environ. Microbiol. 71, 1025–1034.

Dansette, P., Azerad, R., 1974. The shikimate pathway : II. Stereospecificity of hydrogen transfer catalyzed by NADPH-dehydroshikimate reductase of E. coli. Biochimie 56, 751–755.

del Castillo, T., Duque, E., Ramos, J.L., 2008. A set of activators and repressors control peripheral glucose pathways in Pseudomonas putida to yield a common central intermediate. J. Bacteriol. 190, 2331–2339.

Dvořák, P., Burýšková, B., Popelářová, B., Ebert, B.E., Botka, T., Bujdoš, D., Sánchez-Pascuala, A., Schöttler, H., Hayen, H., de Lorenzo, V., Blank, L.M., Benešík, M., 2024. Synthetically-primed adaptation of Pseudomonas putida to a non-native substrate D-xylose. Nat. Commun. 15, 2666.

Elmore, J.R., Dexter, G.N., Baldino, H., Huenemann, J.D., Francis, R., Peabody, G.L., 5th, Martinez-Baird, J., Riley, L.A., Simmons, T., Coleman-Derr, D., Guss, A.M., Egbert, R.G., 2023. High-throughput genetic engineering of nonmodel and undomesticated bacteria via iterative site-specific genome integration. Sci. Adv. 9, eade1285.

Elmore, J.R., Dexter, G.N., Salvachúa, D., O'Brien, M., Klingeman, D.M., Gorday, K., Michener, J.K., Peterson, D.J., Beckham, G.T., Guss, A.M., 2020. Engineered Pseudomonas putida simultaneously catabolizes five major components of corn stover lignocellulose: Glucose, xylose, arabinose, p-coumaric acid, and acetic acid. Metab. Eng. 62, 62–71.

Elmusa, F., Elmusa, M., 2024. Mini-Review on Coumarins: Sources, Biosynthesis, Bioactivity, Extraction and Toxicology. J. Turk. Chem. Soc. Sect. Chem. 11, 933–944.

Gan, Q., Jiang, T., Li, C., Gong, X., Zhang, J., Desai, B.K., Yan, Y., 2025. De novo biosynthesis of 4,6-dihydroxycoumarin in Escherichia coli. Green Chem. 27, 3064–3076.

Ghouse, S.M., Sinha, K., Bonardi, A., Pawar, G., Malasala, S., Danaboina, S., Mohammed, A., Yaddanapudi, V.M., Supuran, C.T., Nanduri, S., 2023. 6-Aminocoumarin oxime-ether/sulfonamides as selective hCA IX and XII inhibitors: Synthesis, evaluation, and molecular dynamics studies. Arch. Pharm. (Weinheim) 356, e2300316.

Guo, X., Crnovcic, I., Chang, C.-Y., Luo, J., Lohman, J.R., Papinski, M., Bechthold, A., Horsman, G.P., Shen, B., 2018. PokMT1 from the polyketomycin biosynthetic machinery of Streptomyces diastatochromogenes Tü6028 belongs to the emerging family of C-methyltransferases that act on CoA-activated aromatic substrates. Biochemistry 57, 1003–1011.

Hirayama, A., Eguchi, T., Kudo, F., 2013. A single PLP-dependent enzyme PctV catalyzes the transformation of 3-dehydroshikimate into 3-aminobenzoate in the biosynthesis of pactamycin. Chembiochem 14, 1198–1203.

Hirayama, A., Miyanaga, A., Kudo, F., Eguchi, T., 2015. Mechanism-based trapping of the quinonoid intermediate by using the K276R mutant of PLP-dependent 3-aminobenzoate synthase PctV in the biosynthesis of pactamycin. Chembiochem 16, 2484–2490.

Incha, M.R., Thompson, M.G., Blake-Hedges, J.M., Liu, Y., Pearson, A.N., Schmidt, M., Gin, J.W., Petzold, C.J., Deutschbauer, A.M., Keasling, J.D., 2020. Leveraging host metabolism for bisdemethoxycurcumin production in Pseudomonas putida. Metab. Eng. Commun. 10, e00119.

Jiang, K., Yan, Z., Di Bernardo, M., Sgrizzi, S.R., Villiger, L., Kayabolen, A., Kim, B.J., Carscadden, J.K., Hiraizumi, M., Nishimasu, H., Gootenberg, J.S., Abudayyeh, O.O., 2025. Rapid in silico directed evolution by a protein language model with EVOLVEpro. Science 387, eadr6006.

Jung, J.-C., Park, O.-S., 2009. Synthetic approaches and biological activities of 4-hydroxycoumarin derivatives. Molecules 14, 4790–4803.

Kai, Y., Matsumura, H., Inoue, T., Terada, K., Nagara, Y., Yoshinaga, T., Kihara, A., Tsumura, K., Izui, K., 1999. Three-dimensional structure of phosphoenolpyruvate carboxylase: a proposed mechanism for allosteric inhibition. Proc. Natl. Acad. Sci. U. S. A. 96, 823–828.

Kaneko, Y., Wang, A., 2024. Synthesis, acid-base responsive fluorescence, and ion-selectivity of novel π-conjugated polymers containing coumarin unit in the main chain. Polymer (Guildf.) 294, 126729.

Kasperkiewicz, K., Ponczek, M.B., Owczarek, J., Guga, P., Budzisz, E., 2020. Antagonists of vitamin K-popular coumarin drugs and new synthetic and natural coumarin derivatives. Molecules 25, E1465.

Koendjbiharie, J.G., van Kranenburg, R., Kengen, S.W.M., 2021. The PEP-pyruvate-oxaloacetate node: variation at the heart of metabolism. FEMS Microbiol. Rev. 45, fuaa061.

Lee, N., Schmidt, M., Li, C., Filbin, C.J., Klass, S., Yaguchi, A., Fear, A.L., Backman, T.W.H., Abel, B.A., Kim, Y.-M., Kim, W.E., Johnson, C.W., Chen, Y., Gin, J.W., Petzold, C.J., Baidoo, E.E.K., Gao, Y., Burnet, M.C., Babnigg, G., Laible, P.D., Singer, C.A., Michener, W.E., Salvachúa, D., Garcia Martin, H., Haushalter, R.W., Keasling, J.D., 2025. Retrobiosynthesis of unnatural lactams via reprogrammed polyketide synthase. Nat. Catal. 8, 389–402.

Li, C., Zou, Y., Jiang, T., Zhang, J., Yan, Y., 2022. Harnessing plasmid replication mechanism to enable dynamic control of gene copy in bacteria. Metab. Eng. 70, 67–78.

Lin, Y., Shen, X., Yuan, Q., Yan, Y., 2013a. Microbial biosynthesis of the anticoagulant precursor 4-hydroxycoumarin. Nat. Commun. 4, 2603.

Lin, Y., Sun, X., Yuan, Q., Yan, Y., 2013b. Combinatorial biosynthesis of plant-specific coumarins in bacteria. Metab. Eng. 18, 69–77.

Ling, J., Horsman, G.P., Huang, S.-X., Luo, Y., Lin, S., Shen, B., 2010. Enediyne antitumor antibiotic maduropeptin biosynthesis featuring a C-methyltransferase that acts on a CoA-tethered aromatic substrate. J. Am. Chem. Soc. 132, 12534–12536.

Ma, Z., Huang, Z., Liao, Y., Mao, J., Yang, J., Dai, Q., Liu, R., Wang, H., Tao, H., Liu, T., 2025. Deciphering the δ-Lactam Formation and lron-Reducing Activity of Spinactins from Saccharopolyspora spinosa. Org. Lett. 27, 565–570.

Manoli, M.-T., Nogales, J., Prieto, A., 2022. Synthetic control of metabolic states in Pseudomonas putida by tuning polyhydroxyalkanoate cycle. MBio 13, e0179421.

Montersino, S., Orru, R., Barendregt, A., Westphal, A.H., van Duijn, E., Mattevi, A., van Berkel, W.J.H., 2013. Crystal structure of 3-hydroxybenzoate 6-hydroxylase uncovers lipid-assisted flavoprotein strategy for regioselective aromatic hydroxylation. J. Biol. Chem. 288, 26235–26245.

Montersino, S., van Berkel, W.J.H., 2012. Functional annotation and characterization of 3-hydroxybenzoate 6-hydroxylase from Rhodococcus jostii RHA1. Biochim. Biophys. Acta 1824, 433–442.

Raj, V., Lee, J., 2020. 2H/4H-chromenes-A versatile biologically attractive scaffold. Front. Chem. 8, 623.

Saadati, F., Modarresi Chahardehi, A., Jamshidi, Negar, Jamshidi, Nazanin, Ghasemi, D., 2024. Coumarin: A natural solution for alleviating inflammatory disorders. Curr. Res. Pharmacol. Drug Discov. 7, 100202.

Sadan, S., Shanmugam, P., Pillai, Z.S., 2025. Advances in 4-hydroxycoumarin chemistry: Functionalization, prominent 4-hydroxycoumarin-based therapeutics and their pharmacological significance. Mini Rev. Med. Chem. 26.

https://doi.org/10.2174/0113895575412635251009051729
Samanth, M., Bhat, M., 2024. Synthesis and importance of coumarin derivatives in medicinal chemistry: A comprehensive review. Russ. J. Bioorganic Chem. 50, 1672–1691.
Schmidt, M., Lee, N., Zhan, C., Roberts, J.B., Nava, A.A., Keiser, L.S., Vilchez, A.A., Chen, Y., Petzold, C.J., Haushalter, R.W., Blank, L.M., Keasling, J.D., 2023. Maximizing heterologous expression of engineered type I polyketide synthases: Investigating Codon optimization strategies. ACS Synth. Biol. 12, 3366–3380.
Schormann, N., Hayden, K.L., Lee, P., Banerjee, S., Chattopadhyay, D., 2019. An overview of structure, function, and regulation of pyruvate kinases. Protein Sci. 28, 1771–1784.
Segars, L.W., Gales, B.J., 1992. Mesalamine and olsalazine: 5-aminosalicylic acid agents for the treatment of inflammatory bowel disease. Clin. Pharm. 11, 514–528.
Sharifi-Rad, J., Cruz-Martins, N., López-Jornet, P., Lopez, E.P.-F., Harun, N., Yeskaliyeva, B., Beyatli, A., Sytar, O., Shaheen, S., Sharopov, F., Taheri, Y., Docea, A.O., Calina, D., Cho, W.C., 2021. Natural coumarins: Exploring the pharmacological complexity and underlying molecular mechanisms. Oxid. Med. Cell. Longev. 2021, 6492346.
Shen, X., Mahajani, M., Wang, J., Yang, Y., Yuan, Q., Yan, Y., Lin, Y., 2017. Elevating 4-hydroxycoumarin production through alleviating thioesterase-mediated salicoyl-CoA degradation. Metab. Eng. 42, 59–65.
Singh, N., Lane, S., Yu, T., Lu, J., Ramos, A., Cui, H., Zhao, H., 2025. A generalized platform for artificial intelligence-powered autonomous enzyme engineering. Nat. Commun. 16, 5648.
Smanski, M.J., Yu, Z., Casper, J., Lin, S., Peterson, R.M., Chen, Y., Wendt-Pienkowski, E., Rajski, S.R., Shen, B., 2011. Dedicated ent-kaurene and ent-atiserene synthases for platensimycin and platencin biosynthesis. Proc. Natl. Acad. Sci. U. S. A. 108, 13498–13503.
Tang, Y., Wang, Y., Guo, X., Xu, Y., Wang, Z., Wu, J., 2024. Recent advances of coumarin-type compounds in discovery of pesticides. J. Agric. Food Chem. 72, 26057–26073.
Tilley, A., McHenry, M.P., McHenry, J.A., Solah, V., Bayliss, K., 2023. Enzymatic browning: The role of substrates in polyphenol oxidase mediated browning. Curr. Res. Food Sci. 7, 100623.
Ullrich, R., Hofrichter, M., 2007. Enzymatic hydroxylation of aromatic compounds. ChemInform 38. https://doi.org/10.1002/chin.200735261
Van Lanen, S.G., Oh, T.-J., Liu, W., Wendt-Pienkowski, E., Shen, B., 2007. Characterization of the maduropeptin biosynthetic gene cluster from Actinomadura madurae ATCC 39144 supporting a unifying paradigm for enediyne biosynthesis. J. Am. Chem. Soc. 129, 13082–13094.
Vargas-Soto, F.A., Céspedes-Acuña, C.L., Aqueveque-Muñoz, P.M., Alarcón-Enos, J.E., 2017. Toxicity of coumarins synthesized by Pechmann-Duisberg condensation against Drosophila melanogaster

643 larvae and antibacterial effects. Food Chem. Toxicol. 109, 1118–1124.
644 Vlachou, E.-E.N., Fotopoulos, I., Gabriel, C., Pontiki, E., Hadjipavlou-Litina, D.J., Litinas, K.E., 2022.
645 Synthesis and biological evaluation of fused dipyranoquinolinones as inhibitors of
646 acetylcholinesterase with antioxidant properties. Eur. J. Med. Chem. Rep. 5, 100063.
647 Vogel, A., 1820. Darstellung von Benzoesäure aus der Tonka‐Bohne und aus den Meliloten ‐ oder
648 Steinklee ‐ Blumen. Ann. Phys. 64, 161‐166.
649 Waldman, A.J., Pechersky, Y., Wang, P., Wang, J.X., Balskus, E.P., 2015. The cremeomycin biosynthetic
650 gene cluster encodes a pathway for diazo formation. Chembiochem 16, 2172–2175.
651 Wang, J., Li, C., Zou, Y., Yan, Y., 2020. Bacterial synthesis of C3-C5 diols via extending amino acid
652 catabolism. Proc. Natl. Acad. Sci. U. S. A. 117, 19159–19167.
653 Yu, S., Plan, M.R., Winter, G., Krömer, J.O., 2016. Metabolic engineering of Pseudomonas putida
654 KT2440 for the production of para-Hydroxy benzoic acid. Front. Bioeng. Biotechnol. 4, 90.
655 Zhang, H., Stephanopoulos, G., 2016. Co-culture engineering for microbial biosynthesis of 3-amino-
656 benzoic acid in Escherichia coli. Biotechnol. J. 11, 981–987.
657 Zhao, H., Xu, Y., Lin, S., Spain, J.C., Zhou, N.-Y., 2018. The molecular basis for the intramolecular
658 migration (NIH shift) of the carboxyl group during para-hydroxybenzoate catabolism. Mol.
659 Microbiol. 110, 411–424.